Supplementary Information

Self-rotating Solar Evaporator for Continuous and Efficient Desalination from Hypersaline Brine

Yun Xia[a], Yang Li[a], Shi Yuan[a], Yuan Kang[a], Meipeng Jian[a], Qinfu Hou[a], Li Gao[b,*], Huanting Wang[a] and Xiwang Zhang[a,*]

[a] Department of Chemical Engineering, Monash University, Clayton, VIC, 3800, Australia.

[b] South East Water Corporation, Seaford, VIC, 3198, Australia.

* Correspondence: xiwang.zhang@monash.edu (X.Z.), li.gao@sew.com.au (L.G.)

1. Material and Methods

1.1. Materials

Carbon nanotubes (CNTs) was bought from Chengdu Organic Chemicals Co. Ltd. and used without further treatment. The polyvinyl alcohol (PVA) cloth was supplied by the Oates Company and purchased from a local grocery store. The cylindrical expanded polyethylene (EPE) foam was supplied by the MORODAY company. All the chemicals were supplied by the Sigma-Aldrich Pty Ltd and used as received, including sodium dodecylbenzene sulfonate (SDBS, flakes), Sodium Chloride (>99.5%), Calcium chloride (≥98%).

1.2. Preparation of the CNTs dispersion

The process for preparing CNTs dispersion was the same as we reported before[1]. Briefly, 100 mg of CNTs and 1000 mg of SDBS were added in 100 ml deionized water (resistivity 18 MΩ·cm). To get a uniform and stable dispersion, a probe sonicator (Q500, QSonica Limited Liability Company) was employed to disperse the CNTs for 30 minutes.

1.3. Preparation of the evaporation layer

The evaporation layer was prepared by coating the CNTs on the PVA cloth. Before started, the PVA cloth was thoroughly cleaned with DI water for a few cycles and dried in an oven at 60 °C. The dry PVA cloth was then soaked in the CNTs dispersion and squeezed for several times to make sure the complete absorption of water. Afterwards, the PVA cloth was taken out and the excess solution was removed with a paper towel. Then the wet PVA cloth was dried in the oven at 60 °C for over 6 hours. Lastly, the coated PVA cloth was then washed with DI water until the washing water is clear.

1.4. Assemble of the rotatable evaporator

First, the EPE cylinder and the CNTs coated PVA cloth were tailored into a suitable dimension. As illustrated in Fig. 2a, the cloth was wrapped around the EPE cylinder. A thin layer of glue (Selleys ShoeFix) was then applied between the cloth and cylinder to binding them together. Afterwards, the whole device was placed in an oven at 60°C for drying.

1.5. Solar evaporation test

The solar evaporation performance was tested with a 150 W Xenon light source (66912, Newport Corporation). Before starting, the solar simulator was adjusted to a suitable intensity via calibrating with a light metre (843-R-USB, Newport Corporation). As the photothermal effect is a full spectral response, a thermopile sensor (919P-010-16, Newport Corporation) with the detecting range between 190 to 11000 nm was selected. To make the adjustment more accurate, five separated spot was measured and then averaged. The temperature change of the evaporator was measured by an infrared camera (TI100, Fluke Pty Ltd) and analysed by SmartView® Infrared Imaging Analysis and Reporting Software. An electronic balance (FZ-300i, A&D Weighing) was employed to record the mass profile of the whole container every 10 seconds. All the experiments were conducted in a windless environment with the room temperature around 23°C and relative humidity of around 50%. A specially designed vessel, which fits the shape of the evaporator (**Fig. S17**), was employed to minimise the inaccuracy

from the uncovered water surface. The desalinated water was collected with the device demonstrated in **Fig. S18**.

1.6. Solar-vapour conversion efficiency

The solar-to-vapour conversion efficiency (η) is defined as:

$$\eta = \frac{\dot{m}_e \Delta h_{lv}}{q_{in}} \qquad \text{Equation (1)}$$

where $\dot{m}_e$ is the as measured water evaporation rate, Δh_{lv} is the latent heat of water vaporization and q_{in} is incident light intensity. As suggested in the literature[2], the evaporation rate in the dark environment is not subtracted as the temperature of the evaporator is higher than the environment.

1.7. Porosity of the PVA cloth

As the PVA cloth is used for water transport, one good way to get effective porosity is to measure the water adsorption. First, a square PVA cloth (dimension: $l \times w$) was cut and its weight was measured (m_1). Then, the PVA cloth was soaked in DI water for over 1 hour. After full absorption, the wet PVA cloth was taken out and the excess water on the surface was scraped off at the edge of a glass beaker. The weight of wet PVA cloth was measured (m_2). The effective porosity of the PVA cloth (Φ) can be calculated as below:

$$\Phi = \frac{(m_2 - m_1)/\rho_w}{l \times w \times d + (m_2 - m_1)/\rho_w} \qquad \text{Equation (2)}$$

Where ρ_w is the density of water (0.997 g cm^{-3}); d is the thickness of the wet PVA cloth.

1.8. Preparation of the spherical evaporator

The spherical evaporator is composed of a central floater, light-absorbing layer and water-transport layer. Expanded polystyrene beads were used as the central floater. The coating ink containing 20 mg ml^{-1} CNTs and 2.5% Nafion in ethanol was used to coat the photothermal material on the central floater by dip-coating method. After uniformly attaching the coating

dispersion, these black beads were then put in the oven at 60°C for 30 min to evaporate the ethanol and stabilize the coating layer. Finally, the hydrophilic polydopamine (PDA) layer was coated with the classic wet coating method[3]. Briefly, the as-obtained CNTs-coated EPS beads were firstly mixed with 50 ml aqueous solution containing 2 mg ml^{-1} dopamine hydrochloride by continuous stirring. Then 60.5 mg Tris·HCl was added into the mixture to initiate the reaction. After reacting for 24 hours, the spherical evaporators were rinsed by the water and then dried in in oven at 60°C for 30 min.

1.9. Preparation of balsa wood evaporator

A round balsa wood log with 19 mm in diameter was cut along the radial direction for 30 mm. The wood cylinder was then pressed on a hot plate at 500 °C to carbonize its side surface[4,5]. To make sure the uniform carbonization, the contact time was controlled to 20 s on each side and then rotate to the neighbouring surface. This process was repeated until the entire side surface turned into a uniform black colour. After carbonization, compressed air was applied to remove the loosely combined carbon particles.

2. Supplementary Figures

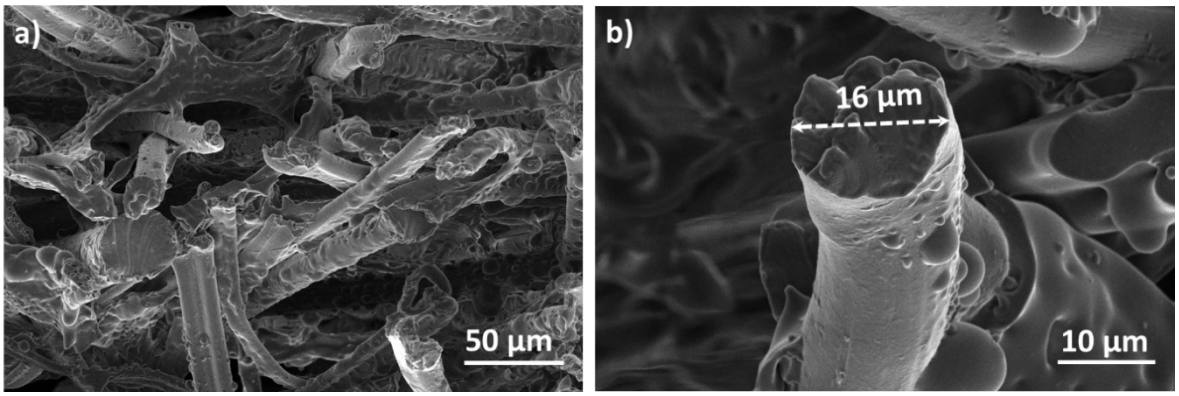

Fig. S1 *a) SEM image of the cross section of the pristine PVA cloth. It is composed of randomly stacked microfibers and PVA polymer around the fibres. b) SEM image of a cutting-off microfiber. The diameter of the microfiber is around 16 µm.*

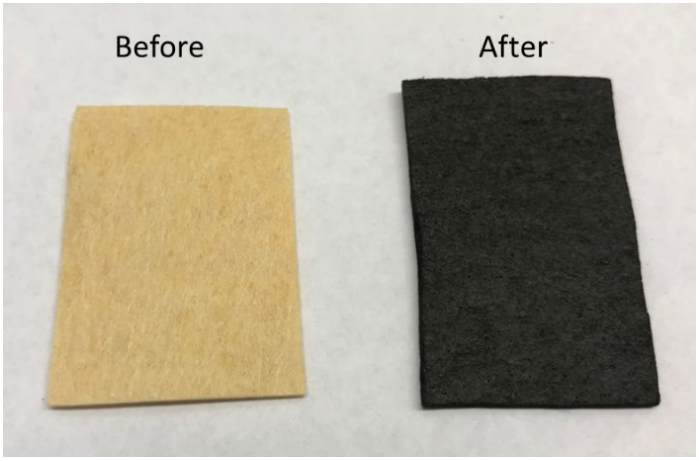

Fig. S2 *Digital photograph of the pristine PVA cloth (a) and after coating with CNTs (b). The PVA cloth turned from yellow to extreme black after the coating process.*

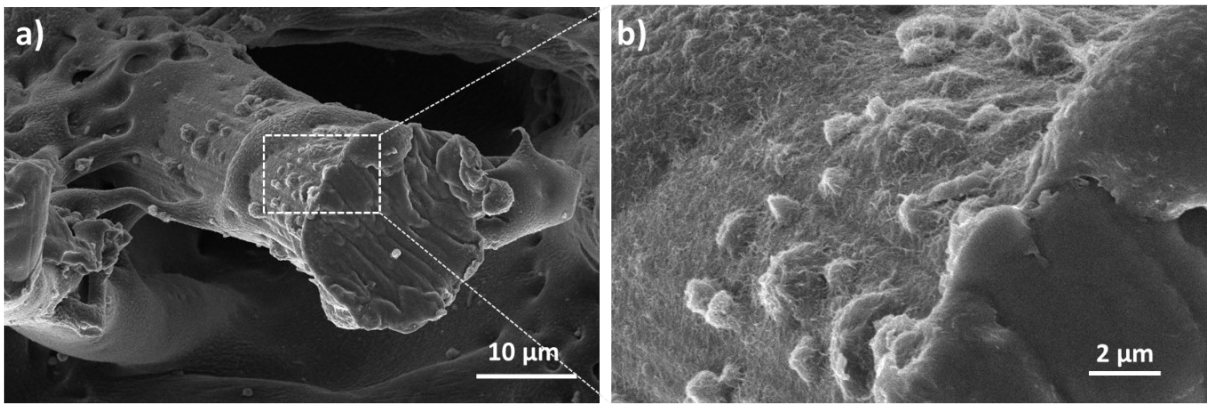

Fig. S3 *a) SEM image of the cross-section of a microfiber. b) enlarged view of the white square area in a). A great amount of CNTs fibres attached on the outer layer of the microfiber.*

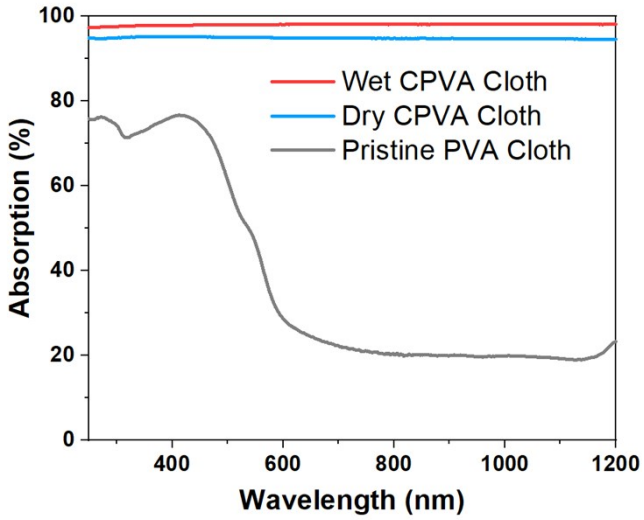

Fig. S4 *Light absorption profiles of the pristine PVA cloth, dry CPVA cloth and wet CPVA cloth.*

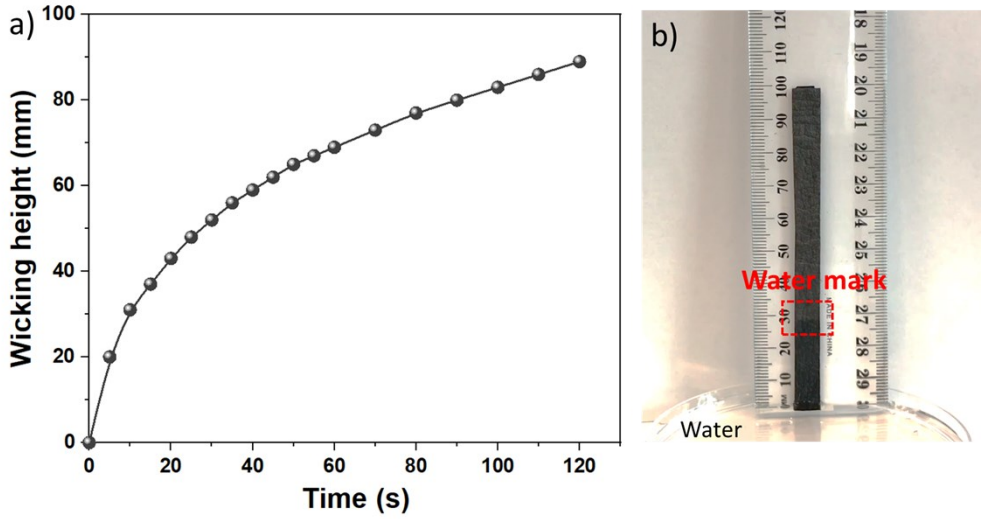

Fig. S5 *a) Wicking-up height of water by the CPVA cloth as a function of time. The fast increase reveals the outstanding water transportability of the CPVA cloth. b) Experimental setup for the water wick-up rate measurement.*

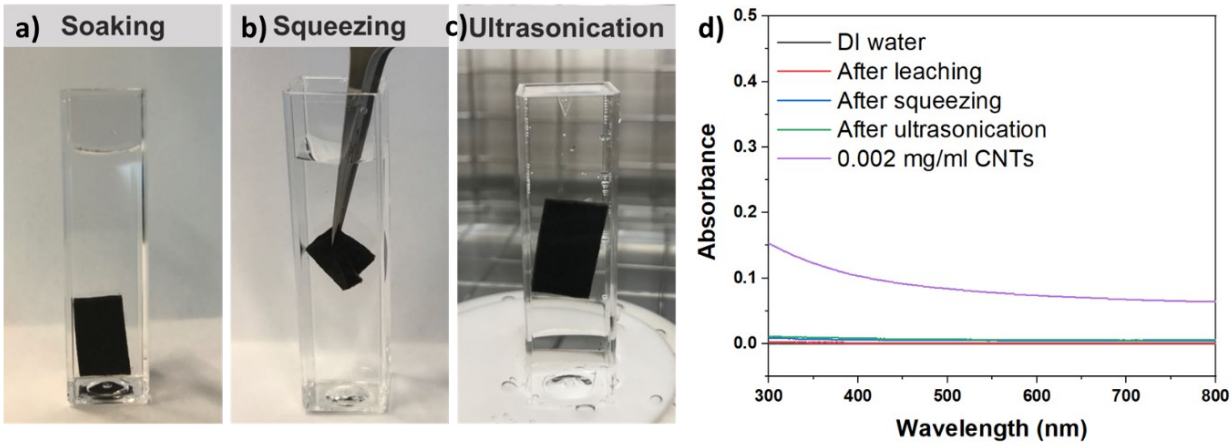

Fig. S6 *Photograph of the residual water after a) soaking, b) squeezing and c) ultrasonication. d) Light absorption of the residual solution after various test condition. The light absorption of DI water and 0.002 mg ml^{-1} CNTs dispersion is also listed as references. The light absorption of the residual solution after leaching, squeezing and ultrasonication is very close the DI water and far below the values of 0.002 mg ml^{-1} CNTs dispersion, revealing the stable bindings between CNTs and PVA cloth.*

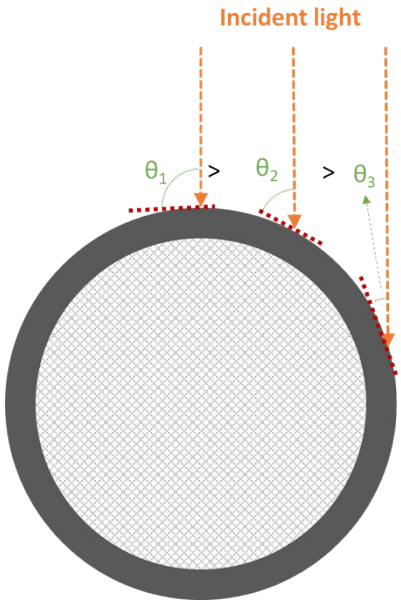

Fig. S7 *Illustration of the non-uniform light irradiation on the cylindrical evaporator. Solar light reaches the top surface of the evaporator perpendicularly (θ_1=90°). The incident angle becomes smaller from the top part to the side surface.*

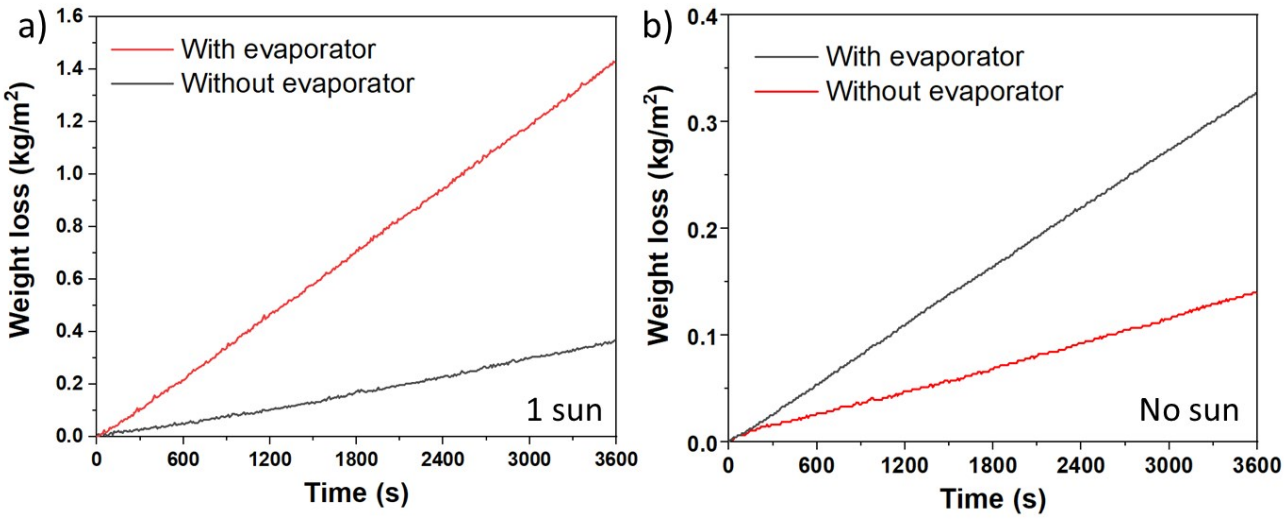

Fig. S8 *a) The weight loss profile with and without the solar evaporator under one sun irradiation. b) The weight loss profile with and without the evaporator in the dark condition.*

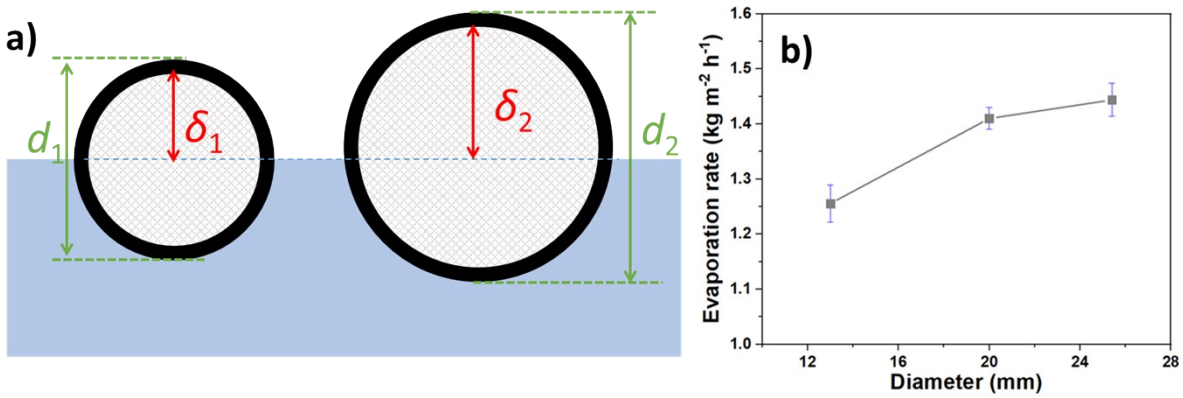

Fig. S9 *Effect of the evaporator diameter on the evaporation performance. a) Illustration of the increasing thickness of insulating foam with larger diameter. b) The evaporation rate with varying rod diameter.*

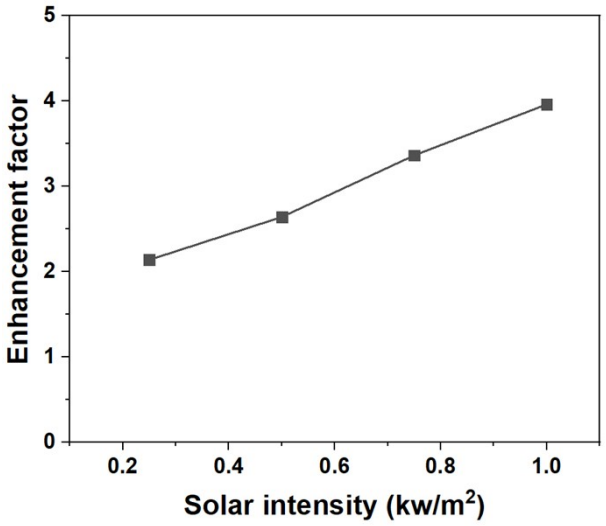

Fig. S10 *The enhancement factor of evaporation rate under different solar intensity. The enhancement factor increases with solar intensity.*

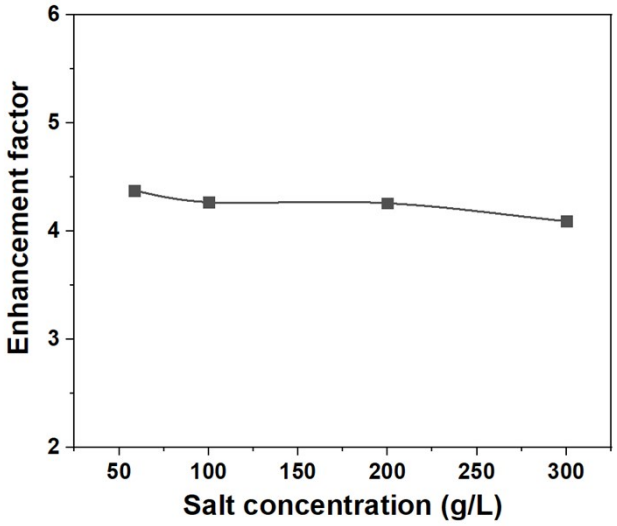

Fig. S11 *The enhancement factor with different salt concentration under one sun.*

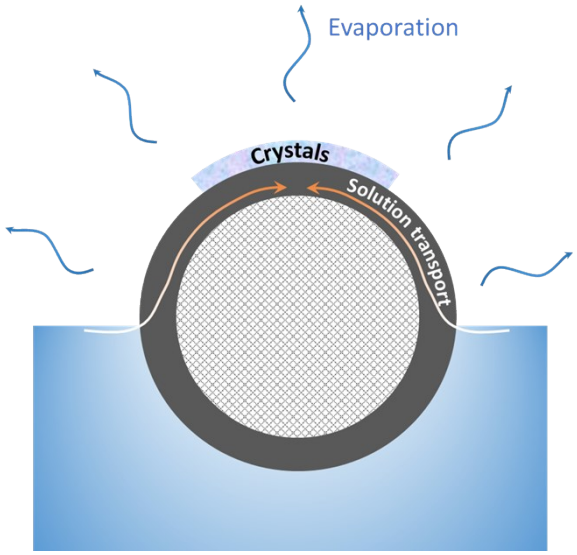

Fig. S12 *Illustration of mass transfer in the rotatable evaporator. Firstly, the solution is wicked up along the PVA cloth from the bottom to the top. During the transport, water continuously evaporates away from the evaporation layer while the salts remain in the brine. Last, the salts become saturated and crystalize out at the top of the evaporator.*

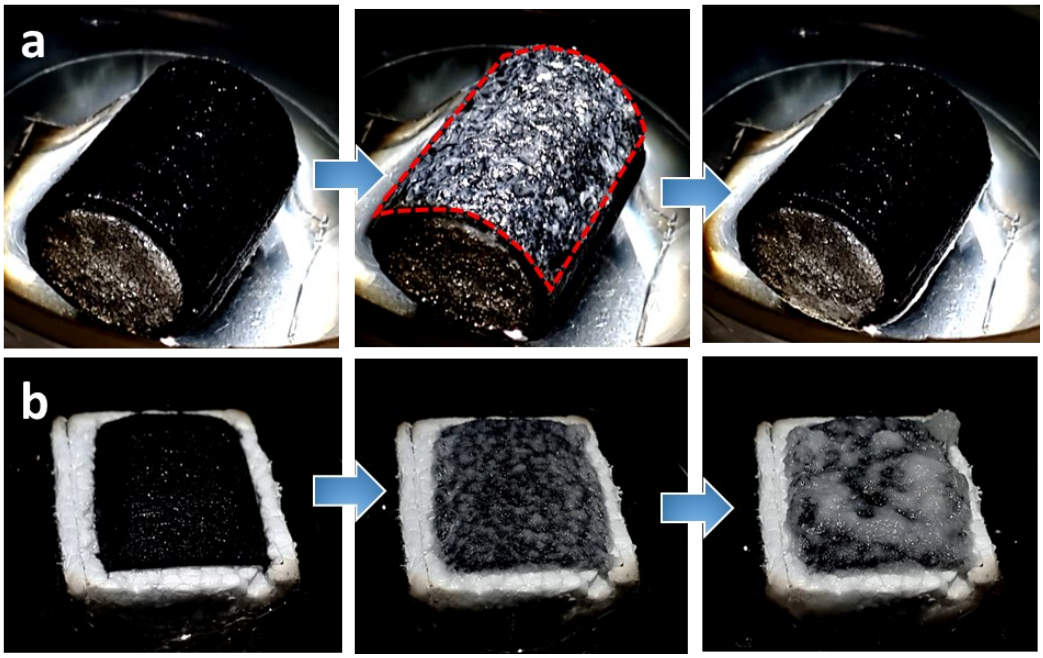

Fig. S13 *a) Performance of the rotatable evaporator dealing with NaCl and $CaCl_2$ mixed solution. With time going on, salts crystals started to cover the surface of the evaporator. After accumulation, the evaporator turned upside-down and exposed a crystal-free surface. b) Performance of the fixed evaporator dealing with NaCl and $CaCl_2$ mixed solution. Salt crystals started to occur and gradually cover the evaporation surface. With time going on, the salt precipitation became more severe and formed a hard crystal layer.*

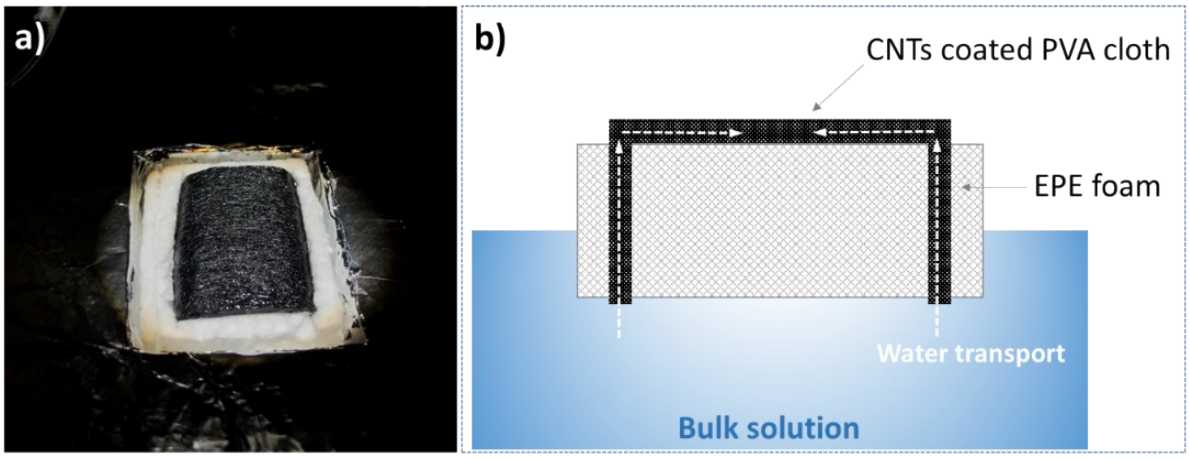

Fig. S14 *a) photograph of the fixed evaporator. a) The schematic of the non-rotatable flat solar absorber.*

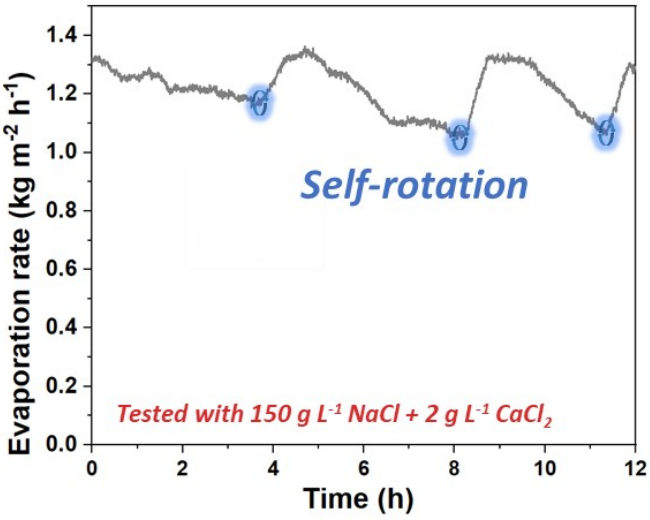

Fig. S15 *Evaporation profile with 150 g L^{-1} NaCl and 2 g L^{-1} $CaCl_2$.*

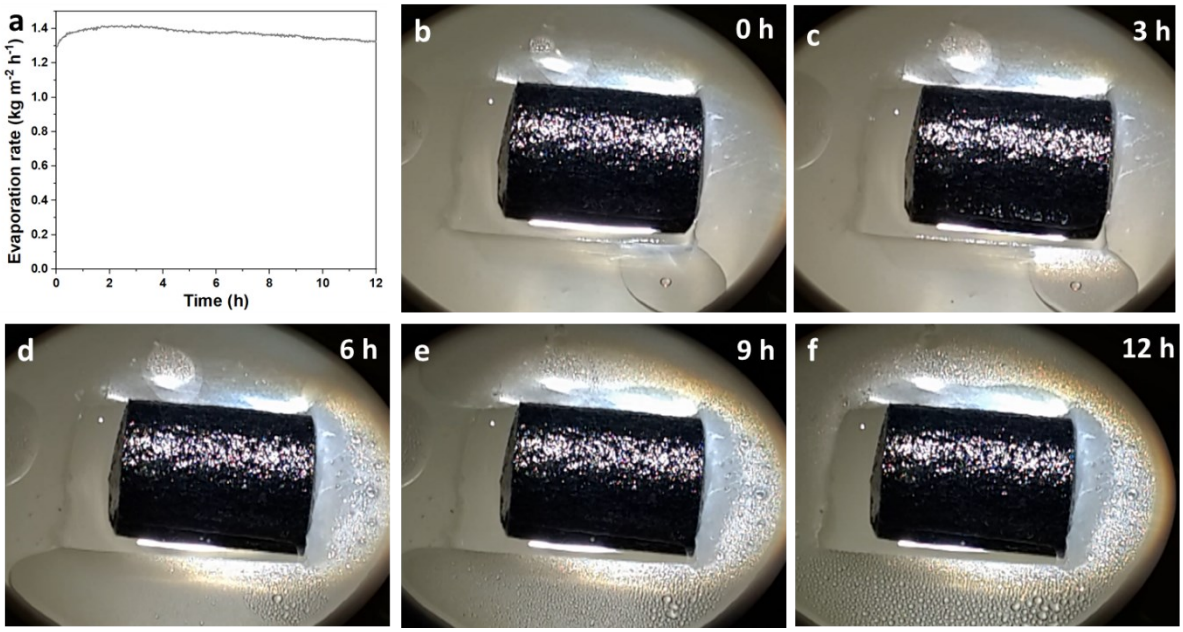

Fig. S16 *Desalination performance with 35 g L^{-1} NaCl solution. a) Water evaporation rate during the 12 hour testing period. b)-f) Photograph of the evaporator at 0 h, 3h, 6 h, 9h and 12 h, respectively.*

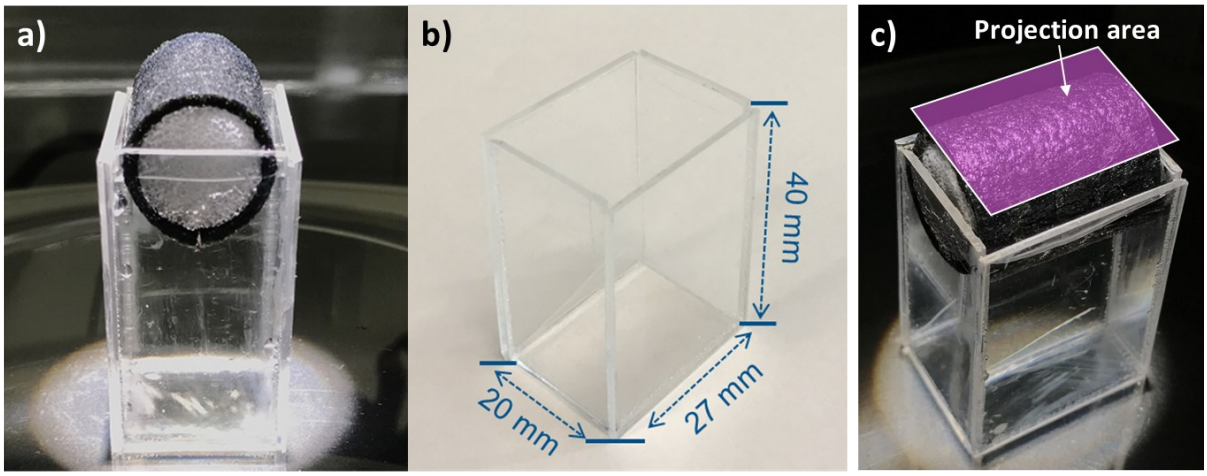

Fig. S17 *a) Experimental setup for the water evaporation rate testing. To avoid evaporation from the uncovered water surface, a homemade container was employed to fit the projecting area of the evaporator. b) Dimension of the homemade testing container. c) The area for evaporation rate measurement*

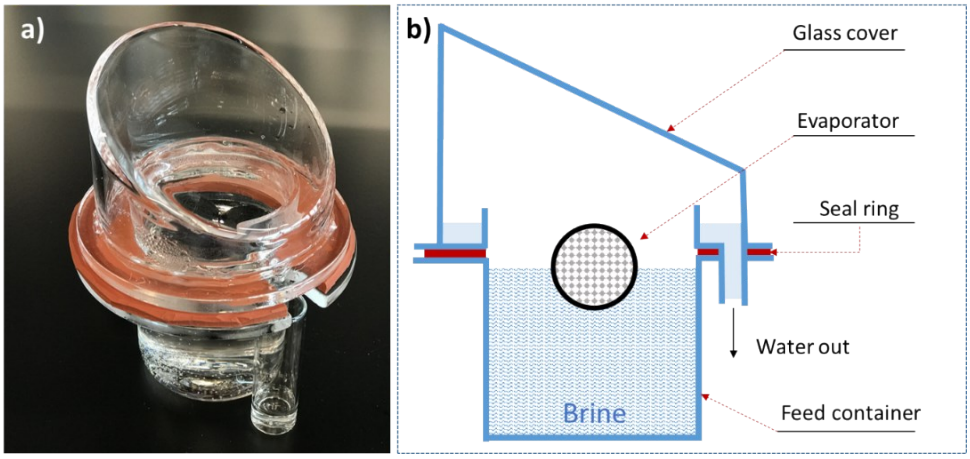

Fig. S18 *Experimental setup for water collection. A) The digital photograph and b) the design scratch*

3. Supplementary Table

Table S1 *Comparison of evaporation performance with other literatures that achieved continuous operation for brine solution*

Material/device	Light intensity (kW m^{-2})	NaCl Concentration (g L^{-1})	Evaporation rate (kg m^{-2} h^{-1})	Efficiency
Bimodal porous solar evaporator[5]	1	166.0	0.80	57.0%
	6	166.0	6.40	78.0%
Channel-array Carbonized wood[6]	1	229.1	1.04	75.0%
Flexible graphite film[7]	0.75	166.0	0.61	38.2%
	1	166.0	1.01	62.7%
Waterlily–inspired evaporator[8]	1	106.9	1.28	78.5%
Salt harvesting disc[1]	1	58.5	1.00	68.0%
	1	150	0.98	66.9%
Low tortuosity Janus evaporator[9]	1	73.3	1.25	83.3%
	1	130.0	1.22	81.8%
Current work	1	100	1.38	86.6%
	1	200	1.26	79.1%
	1	300	1.15	72.2%

4. Reference

1 Y. Xia, Q. Hou, H. Jubaer, Y. Li, Y. Kang, S. Yuan, H. Liu, M. W. Woo, L. Zhang, L. Gao, H. Wang and X. Zhang, *Energy Environ. Sci.*, 2019, **12**, 1840–1847.

2 X. Li, G. Ni, T. Cooper, N. Xu, J. Li, L. Zhou, X. Hu, B. Zhu, P. Yao and J. Zhu, *Joule*, 2019, **3**, 1798–1803.

3 H. Lee, S. M. Dellatore, W. M. Miller, P. B. Messersmith and P. B. Lee, H., Dellatore, S.M., Miller, W.M. and Messersmith, *Science (80-.).*, 2007, **318**, 426–430.

4 M. Zhu, Y. Li, G. Chen, F. Jiang, Z. Yang, X. Luo, Y. Wang, S. D. Lacey, J. Dai, C. Wang, C. Jia, J. Wan, Y. Yao, A. Gong, B. Yang, Z. Yu, S. Das and L. Hu, *Adv. Mater.*, 2017, **29**, 1704107.

5 S. He, C. Chen, Y. Kuang, R. Mi, Y. Liu, Y. Pei, W. Kong, W. Gan, H. Xie, E. Hitz, C. Jia, X. Chen, A. Gong, J. Liao, J. Li, Z. J. Ren, B. Yang, S. Das and L. Hu, *Energy Environ. Sci.*, 2019, **12**, 1558–1567.

6 Y. Kuang, C. Chen, S. He, E. M. Hitz, Y. Wang, W. Gan, R. Mi and L. Hu, *Adv. Mater.*, 2019, **31**, 1900498.

7 V. Kashyap, A. Al-Bayati, S. M. Sajadi, P. Irajizad, S. H. Wang and H. Ghasemi, *J. Mater. Chem. A*, 2017, **5**, 15227–15234.

8 N. Xu, J. Li, Y. Wang, C. Fang, X. Li, Y. Wang, L. Zhou, B. Zhu, Z. Wu, S. Zhu and J. Zhu, *Sci. Adv.*, 2019, **5**, eaaw7013.

9 R. Hu, J. Zhang, Y. Kuang, K. Wang, X. Cai, Z. Fang, W. Huang, G. Chen and Z. Wang, *J. Mater. Chem. A*, 2019, **7**, 15333–15340.